Monthly Notices
of the
ROYAL ASTRONOMICAL SOCIETY

MNRAS **428,** 2949–2965 (2013) doi:10.1093/mnras/sts238

The transmutation of dwarf galaxies: stellar populations

Mina Koleva,[1,2]★ Antoine Bouchard,[3] Philippe Prugniel,[2] Sven De Rijcke[1] and Isabelle Vauglin[2]

[1]*Sterrenkundig Observatorium, Ghent University, Krijgslaan 281, S9, B-9000 Ghent, Belgium*
[2]*Université Lyon 1, Villeurbanne, F-69622; CRAL, Observatoire de Lyon, St. Genis Laval, F-69561; CNRS, UMR 5574, France*
[3]*Department of Physics, McGill University, Montreal, QC H3A 2T8, Canada*

Accepted 2012 October 17. Received 2012 October 12; in original form 2012 August 8

ABSTRACT

Transition-type dwarf (TTD) galaxies share characteristics of early- and late-type dwarfs. Thus, they are suspected to be the thread that connects them. We selected 19 TTD galaxies in the nearby Universe ($cz < 2900$ km s^{-1}) from the Sloan Digital Sky Survey. They span the luminosity range from $\sim-$ 14.5 to -19.0 mag in the B band, and are located in different environments.

We derive their single stellar population parameters and star formation histories, using the full spectrum fitting technique with two independent population synthesis models. Irrespective of the synthesis models, we find that these dwarfs have a relatively young mean age (around 1–2 Gyr) and low metallicities ($\sim-$ 0.7 dex). Moreover, they had approximately constant star formation rates until a few Gyr ago, associated with strong metal enrichment during the first few Gyr of their evolution. We compare these results with the results from Koleva et al., who studied dwarf elliptical (dE) galaxies in the same luminosity range. We find that (1) both samples occupy the same region in the luminosity–metallicity relation, (2) the build-up of the stellar mass in both types of galaxies is very similar, with most of the stars already formed 5 Gyr ago and (3) contrary to the dEs, TTDs are forming stars at present, but after 1 Gyr of passive evolution, their star formation histories would appear identical to that of dEs.

As far as the stellar population is concerned, the transformation of TTDs into dEs is definitely possible. A star-forming dwarf galaxy can be stripped of at least a fraction of its gas, and its star formation rate can be reduced to that of the TTDs of the present sample. Continued gas removal may drive a galaxy to the state of a gas-depleted bona fide dE. However, we cannot exclude a scenario where a star-forming galaxy is rapidly transformed into an early type without passing through a noticeable 'transition' phase, as suggested by the relatively small fraction of observed dEs with an interstellar medium. We cannot exclude swinging back and forth between a late-type dwarf and a TTD (in the case of episodic star formation) or an early-type dwarf and a TTD (in the case of gas infall).

Key words: galaxies: dwarf – galaxies: evolution – galaxies: formation – galaxies: stellar content.

1 INTRODUCTION

Dwarf galaxies can be broadly divided into star-forming systems with substantial amounts of cold gas ($M_{\rm H\,I}/L_B > 0.2$; Dellenbusch et al. 2008 and references therein) and quiescent, gas-depleted galaxies with smooth isophotes. The former class includes dwarf irregular (dIrr) and blue compact dwarf (BCD) galaxies, while the latter consists of dwarf elliptical (dE) and dwarf spheroidal (dSph) galaxies. Evolutionary connections between the present-day star-forming and quiescent galaxies have not only been long suspected (Sandage & Binggeli 1984) but also challenged (e.g. Grebel, Gallagher & Harbeck 2003). The existence of an intermediate class of dwarfs [transition-type dwarf (TTD) galaxies] supports the evolutionary connections.

TTD galaxies can be broadly defined as objects bearing characteristics of both irregular and elliptical galaxies. Some of them appear as dE galaxies in optical wavelengths, but contain some H I gas (Conselice et al. 2003; Bouchard et al. 2005; Buyle et al. 2005; Beaulieu et al. 2006; di Serego Alighieri et al. 2007; Grossi et al. 2007, 2009). They do not show prominent signs of ongoing or recent star formation. Others display vigorous star formation,

★ E-mail: mina.koleva@ugent.be

like dIrr galaxies, but regular external isophotes reminiscent of dEs (Sandage & Hoffman 1991; Knezek, Sembach & Gallagher 1999; Dellenbusch et al. 2008). Finally, some have a hot interstellar medium (ISM) indicative of residual star formation (Sandage & Fomalont 1993; De Rijcke et al. 2003; Michielsen et al. 2004; Lisker et al. 2006; Bouchard et al. 2010). Note finally that some nearby bona fide dEs, namely NGC 185 and NGC 205, show a mild star formation in their centre. This is quantitatively compatible with the local gas supplied by the stellar evolution (Davidge 2003) and may be common in dEs but undetected because of the small size of the star-forming region.

Some TTDs contain relatively small amount of neutral gas ($M_{\rm H\,I}/L_B < 0.1$) compared to dIrrs, but some others contain as much H I as dIrr galaxies (Bouchard, Da Costa & Jerjen 2009). While the latter may resume an active star formation, and swing back to a dIrr/BCD phase, the former lacks the potential of reaching high star formation rates (SFRs) and may be evolving towards dE, possibly because their original gas reservoir has been partially stripped.

Dellenbusch, Gallagher & Knezek (2007) measured the oxygen abundances of H II region in five Sandage–Hoffman type TTDs with $M_B \sim -18$ mag. They found that in general those galaxies lie above the luminosity–metallicity relation for star-forming dwarfs. Their first hypothesis was that these TTDs are recent mergers, but a further photometric study by Dellenbusch et al. (2008) did not reveal any disturbance in their profiles, like tidal stellar tails. They concluded that most probably their TTDs are BCDs in the end of the active lifetime, fading away.

Sánchez Almeida et al. (2009) analysed stacked Sloan Digital Sky Survey (SDSS) spectra of ∼21 500 quiescent BCDs (QBCDs, according to their nomenclature) with $-18 \lesssim M_B \lesssim -13$ mag. These galaxies match our present definition for TTDs; they have 'red' body ($0.5 \leq M_{\rm g} - M_{\rm r} \leq 1.1$ mag, i.e. redder than a BCD) with little (or no) star formation. Dellenbusch et al. (2007) observe that the oxygen abundances of the QBCDs are larger than that of the BCDs. The authors argue that this difference can be explained with the longer mixing time-scales. In other words, the observed metallicities are representative of the H II regions before the dilution within the galactic gas reservoir. This statement is supported by the fact that the stellar metallicity of their QBCDs is consistent with the gas metallicity of the BCDs.

Weisz et al. (2011) derived the star formation histories (SFHs) of 60 star-forming, quiescent and transition-type dwarfs from the ANGST sample[1] (Dalcanton et al. 2009). The dwarfs span almost 10 mag in luminosities, with M_B from −8.49 to −16.57 mag. Irrespective of their present morphology, their average SFHs are identical for most of the Hubble time, with the difference being only in the last few Gyr. All ANGST dwarfs seem to have formed half of their mass by $z \sim 2$, again independent of their present morphology.

In the vicinity of the Milky Way, a few galaxies have mixed morphologies. Even fewer have deep, photometric observations, reaching the oldest main-sequence turn-off in the colour–magnitude diagram, allowing us to resolve the SFHs at early epochs. Phoenix (Hidalgo et al. 2009) and LGS-3 (Hidalgo et al. 2011) were observed with the *Hubble Space Telescope* Wide Field Planetary Camera 2 (WFPC2) and the Advanced Camera for Surveys (ACS) in the frame of the LCID[2] project. Both have similar SFHs, with an important fraction of the stellar mass being formed in the first few Gyr of their evolution and some residual star formation until now. The metallicity enrichment history is less intuitive. According to the authors the bulk of the stars were formed during the first half of the galactic life, while the star formation was the strongest. In contrast, the residual star formation in the end produced stars with 0.7 dex higher metallicities. The authors argued that a stronger enrichment appears when the star formation is milder and the winds from supernova explosions are weaker. Thus the enriched gas is not expelled to large galactocentric distances, as also observed in simulated dwarfs (Valcke, de Rijcke & Dejonghe 2008; Schroyen et al. 2011; Cloet-Osselaer et al. 2012). Two dSph galaxies of similar luminosity, Cetus and Tucana, were also studied in LCID. Their SFHs remind those of the TTDs, notwithstanding the apparent differences at the earliest epochs (before 12 Gyr). Their metal enrichment is more gentle, but again with some, though milder, offset. Hidalgo et al. (2011) argued that the differences observed between the metal enrichment in dSph and TTDs of similar luminosities may be explained if dSphs had higher masses and experienced stronger tidal stripping at early epochs.

Grebel et al. (2003) have shown that on the metallicity–luminosity relation the TTDs occupy the same region as the dEs for galaxies with stellar masses about 10^7 M$_\odot$. In this paper, we examine the question of the continuity and/or the evolutionary link between the TTDs and the gas-depleted dEs, by analysing their star formation and metal-enrichment histories. While descending the mass sequence we have seen that in general TTDs and fairly massive, late-type dwarfs and TTDs and less massive, early-type dwarfs share identical stellar population properties. However, no detailed comparison has been done to date (at least to the authors' knowledge) between TTDs and dEs with $M_\star \sim 10^9$ M$_\odot$.

Koleva et al. (2009a) have shown that typically 50 per cent of the stellar mass of dEs with $M_\star \sim 10^9$ M$_\odot$ was formed more than 5 Gyr ago. Then, the star formation generally continued to a recent past, and in some cases a residual star formation is observed (see also Lisker et al. 2006). (Those latter objects may possibly be classified as TTDs.) Some dEs display a somewhat constant SFR quenched a few 100 Myr ago, and some others display a rapidly decreasing SFR. The last bursts of star formation were more centrally concentrated, consistent with the observations of the TTDs with active star formation of Dellenbusch et al.

In this paper, using SDSS (York et al. 2000) spectra, we will study the stellar populations in the centre of a sample of TTDs. We will derive single stellar population (SSP) equivalent ages and metallicities, star formation and metal-enrichment histories of these galaxies. We will analyse the SFHs of the TTDs after 1 Gyr of simulated passive evolution. We will compare all these results with the results of analogous analyses of a sample of dEs with similar luminosities and estimate if the evolutionary end product of a TTD could be a dE.

This paper proceeds as follows: in Section 2 we present the sample and the observational material; in Section 3 we describe the analysis method and the derived SFH; Sections 4 and 5 are the discussion and the conclusions, respectively.

2 SAMPLE AND OBSERVATIONAL MATERIAL

We selected dwarf galaxies from the literature, mentioned either for their mixed morphology (irregular star-forming central region and smooth elliptical external isophotes) or for the detection of H I together with a dE appearance. These criteria merely reflect our 'working definition' of a TTD. Multiwavelength observations (radio, optical, etc.), which unfortunately do not exist for the large

[1] http://www.nearbygalaxies.org//dashboard/home
[2] http://rialto.ll.iac.es/proyecto/LCID/

majority of these faint galaxies, might lead to slight differences regarding the classification of some of the objects.

Sandage & Hoffman (1991) introduced NGC 4286 and 3377A as prototypes for the class of mixed-morphology galaxies. Knezek et al. (1999), relating the Hα to the H I emission, estimated that (some) TTDs can sustain star formation for more than a Hubble time and are therefore not likely to passively evolve towards dEs. Still, future environment effects may drive the removal of the gas and their morphological classification. The latter authors classified NGC 4286 as a dwarf spiral and we included it in our sample since it was observed with the SDSS.

Dellenbusch et al. (2008) selected five TTDs with star formation signatures in the centre. Four of them were observed in the SDSS and were accordingly included sample: NGC 3265, NGC 3353, NGC 3928 and IC 745. These galaxies are expected to finish their gas supplies in less than 1 Gyr, providing the same SFRs.

Conselice et al. (2003) detected H I in Virgo dE galaxies and compiled other detections from the literature. We included seven galaxies (from nine detections) observed in the SDSS. di Serego Alighieri et al. (2007) detected H I in 13 early-type galaxies of the Virgo cluster from the ALFALFA survey. Two of these galaxies are bright ellipticals, and six are faint and not observed in the spectroscopic SDSS (VCC 421, VCC 956, VCC 1142, VCC 1202, VCC 1964 and VCC 2062); we included the other five galaxies.

Finally, Grossi et al. (2009) searched for early-type galaxies in ALFALFA outside of the Virgo cluster. Out of the 50 early-type galaxies that they identified in the searched region, and within a radial velocity of 3000 km s^{-1}, they found 15 objects detected in ALFALFA. We excluded NGC 2962, a luminous S0 galaxy, NGC 3489 and NGC 3773 which are not part of the spectroscopic SDSS sample. We included the other 12 in our sample, for nine of them the SDSS spectra have a sufficient signal-to-noise ratio (S/N) for stellar population analyses.

Though the selected sample does not fulfil completeness criteria, it is suited to explore the SFH of these galaxies and determine if they form a homogeneous family. Our sample can be seen as a continuation of the ANGST sample (Dalcanton et al. 2009; Weisz et al. 2011) of nearby dwarf galaxies ($D \lesssim 4$ Mpc). Their brightest TTD is with $M_B = -12.85$, while the faintest galaxy in our sample has $M_B = -14.54$ (VCC 797). The basic characteristics of the 19 galaxies in our compilation are summarized in Table 1.

The luminosities, spanning the range $-19 < M_B < -15$, are between the low-luminosity elliptical galaxies (like NGC 4478) and the 'bright' dE prototype NGC 205 ($M_B \simeq -15.8$) and analogous to the dEs of the sample of Koleva et al. (2009a).

2.1 Environment

The environment is likely to be a key factor for the evolution of dwarf galaxies. It affects the galaxies through ram-pressure stripping and tidal harassment. Therefore, we used the grouping algorithm installed in the HyperLeda data base[3] (Paturel et al. 2003) and described in Prugniel, Golev & Maubon (1999) to add a description of the environment listed in Table 1.

For each target from our sample, the galaxies present in the data base are iteratively grouped on the basis of their proximity in projected distance and radial velocity difference. Table 1 gives the number of galaxies grouped with the target (N_g), the velocity dispersion and radius of this group (σ_g and R_g) and the dimensionless position in the group: $\Delta V = (V_{galaxy} - V_{group})/\sigma_g$ and $\Delta R = R_{galaxy}/R_g$, where R_{galaxy} is the radial position of the galaxy in the group.

Other parametrization of the environment could have been chosen. We could have used either the distance to the cluster/group centre or the distance from the five closest neighbouring galaxies brighter than -19 mag in the B band (Goto et al. 2003). The former parameter assumes that the galactic assembly is symmetrical, while the latter is not suitable for sparsely populated environments, where the massive galaxies are rare. Both parameters would work better if the three-dimensional distribution of the galaxies is known. Moreover, they indicate the present configuration and do not carry information about the orbital history of the galaxies. The adopted parametrization has demonstrated good performance in low-density environments (Prugniel et al. 1999). The derived density correlates with deviations to the Fundamental Plane that reflect differences in the stellar population (Prugniel & Simien 1996).

2.2 Spectroscopic data

We retrieved the spectra from the SDSS data release 7 (DR7[4]; Abazajian & Sloan Digital Sky Survey 2009). The spectrograph, fed by fibres subtending 3 arcsec on the sky, has two arms, with a dichroic filter to separate the blue and red beams at 6150 Å. The processed spectra render the wavelength range from 3800 to 9200 Å, with a full width at half-maximum spectral resolution of $1800 < R = \Delta\lambda/\lambda < 2200$. They are evenly log-wavelength sampled, with a pixel size equivalent to 69 km s^{-1} (i.e. 1.1–1.8 Å pixel^{-1}), and are flux calibrated.

The spectra of the Sandage–Hoffman type galaxies have a reasonable S/N >30, while those of the H I-detected galaxies in the Virgo cluster have generally much lower S/N. The exception is IC 3025 (S/N $\sim$ 20). Only three other H I-detected objects are suited for SFH analyses (NGC 4323, VCC 1949 and VCC 1993) and another one for the determination of SSP-equivalent characteristics (VCC 797). Emission lines are detected in two of the seven 'faint' Virgo H I galaxies that we did not include in the sample. The field H I galaxies are brighter than those of Virgo and their spectra can be used for the population analysis. Although the analysis of the SFH is independent of Galactic extinction, in order to determine the internal extinction using either the Spectral Energy Distribution (SED) or the Balmer decrement we corrected the SDSS spectra for the Galactic extinction. We used the extinction maps of Schlegel, Finkbeiner & Davis (1998) and the extinction law from Schild (1977). The B-band absorption is between 0.03 and 0.1 mag, with an average $\langle A_B \rangle = 0.08$ mag. The sampled galaxies cover distances between 11 and 55 Mpc, hence the SDSS 3 arcsec field of view will correspond to 150–750 pc. Therefore, for most of the galaxies we probe only the inner 1/10th of the galaxy's D_{25} in the B band. The only exception is Mrk 0706, for which we probe roughly half of its size.

3 STELLAR POPULATION STUDIES

To determine the SFH, we fit the spectra against models of stellar populations using a full spectrum fitting method. This consists in comparing, pixel-by-pixel, the spectrum to a model as made in e.g. Mathis, Charlot & Brinchmann (2006), Cid Fernandes et al. (2005) or Asari et al. (2007). In this section we will first describe briefly the method we use and direct the reader to further readings, secondly we

[3] http://leda.univ-lyon1.fr

[4] http://cas.sdss.org/

Table 1. Basic characteristics of the galaxies of the sample computed from the HyperLeda data base (except for the last column). Subsample source – 1: Sandage & Hoffman (1991); 2: Dellenbusch et al. (2008); 3: Conselice et al. (2003); 4: di Serego Alighieri et al. (2007); 5: Grossi et al. (2009). B_t is the B-band total magnitude, not corrected for extinction. M_B is the absolute B-band magnitude computed after correcting B_t for extinction and applying k-correction. M_{H1}/L_B is the H I mass content relative to the luminosity of the galaxy in the B band (taken from the corresponding papers from column 2). D_{25} is the major axis diameter at the 25th B-band isophote. $\epsilon = 1 - b/a$ is the apparent flattening. N_g, σ_g, R_g, ΔV, ΔR describe the environment; they are, respectively, the number of associated galaxies, the velocity dispersion and radius of this group, and the 'position' of the galaxy in the group, in projected velocity and radius. In the notes, 'Em' signals the presence of strong emission lines in the SDSS spectra, and 'Em-' signals the presence of weak emission. The designations of the following galaxies were shortened: SDSS J093608.59+061525.4 and 2MASX J11460404+1134529.

Name	Subsample source	V_{Helio} (km s^{-1})	Distance (Mpc)	B_t (mag)	M_B (mag)	M_{H1}/L_B ($M_\odot/L_\odot$)	D_{25} (arcsec)	D_{25} (kpc)	$\epsilon = 1 - b/a$	N_g	σ_g (km s^{-1})	R_g (Mpc)	ΔV	ΔR	Notes
Sandage–Hoffman type															
NGC 4286	1	643	11.4	14.72	−15.96		65	3.6	0.65	68	257	0.6	0.6	0.1	Em-
NGC 3265	2	1442	28.4	14.04	−18.36	0.10	58	8.0	0.27	13	137	1.3	0.1	0.1	Em
NGC 3353	2	943	23.9	13.23	−18.91	0.30	81	9.4	0.28	161	305	2.1	0.8	1.7	Em
NGC 3928	2	983	19.3	13.16	−18.37	0.33	82	7.6	0.08	100	151	1.5	0.5	0.4	Em
IC 0745	2	1134	21.7	14.11	−17.67	0.05	47	4.9	0.03	64	237	1.5	1.6	0.6	Em
H I-detected dwarf galaxies															
NGC 4323 (VCC 0608)	3	1853	19.4	14.96	−16.62	1.8	74	7.0	0.42	159	308	1.5	2.1	0.8	
VCC 797	3	773	19.4	17.04	−14.54	0.38	30	2.8	0.00	655	698	1.6	0.2	1.3	
VCC 1949 (NGC 4640)	3	1761	19.4	14.34	−17.24	0.38	96	9.1	0.44	655	684	1.6	1.2	0.8	
IC 3025 (VCC 021)	4	485	19.4	14.89	−16.65	0.1	44	4.1	0.41	671	697	1.6	0.6	1.0	
VCC 1993	4	915	19.4	15.41	−16.15	0.13	40	3.7	0.04	654	684	1.6	0.0	0.8	
UGC 04599	5	2098	36.8	15.09	−17.91	0.11	60	10.7	0.08	10	147	2.0	0.3	0.3	Em-
Mrk 0706	5	2489	55.1	16.54	−17.30	0.14	6	1.7	0.12	81	389	4.0	2.0	0.4	Em
SDSS J0936	5	2424	38.3	17.24	−16.37	0.69	22	4.1	0.56	19	225	2.8	1.3	0.2	Em
IC 0676	5	1407	14.1	13.50	−17.37	0.02	111	7.6	0.29	56	351	1.0	1.2	1.0	Em
IC 0692	5	1161	13.9	14.18	−16.74	0.28	46	3.1	0.31	69	266	1.1	0.7	1.2	Em
IC 0719	5	1849	34.9	13.91	−19.06	0.25	73	12.3	0.68	2	67	1.3	1.0	0.0	Em-
UGC 06655	5	739	13.2	14.93	−15.82	0.22	41	2.6	0.38	71	207	1.1	0.9	1.0	Em
2MASX J1146	5	2977	55.4	15.51	−18.33	0.17	42	11.3	0.41	20	182	2.6	1.4	0.8	Em
NGC 5338	5	813	15.6	14.06	−17.03	0.02	116	8.8	0.56	21	173	0.7	2.2	0.1	Em

will present our SSP-equivalent analyses (Section 3.2) and finally we will report our SFH reconstructions using a linear combination of SSPs (Section 3.3).

3.1 Method

In this paper, we are following the procedure used in Koleva et al. (2009a) to study the stellar population of dE galaxies. It uses the ULYSS package (Koleva et al. 2009b) to perform a non-linear χ^2 minimization against a linear combination of SSP models convolved with the internal kinematics of the galaxy and multiplied by a polynomial absorbing the effects of line-of-sight extinction or flux calibration uncertainties.

We use two sets of population models, those of Vazdekis[5] (Vazdekis et al. 2010, v9.1) based on the Miles library (Sánchez-Blázquez et al. 2006) and Pegase-HR[6] (Le Borgne et al. 2004) based on the Elodie 3.2 library (Prugniel & Soubiran 2001; Wu et al. 2011). The two sets of models were shown to be the best presently available, and they were found to be in a good agreement when used to derive SSP-equivalent characteristics (Koleva et al. 2008).

To adjust the population models to the resolution of the SDSS spectra (changing with the wavelength), we followed the recipes of Koleva et al. (2009b). The instrumental broadening (line-spread function) was determined using spectra of stars from the M67 cluster. Wavelengths bluer than 4000 Å were excluded from the fit because they (especially the H&K region) are reproduced poorly by the models (Koleva et al. 2008). The pixels were weighted according to their variance, communicated in the standard SDSS fits' files. We used automatic $\kappa-\sigma$ clipping to exclude the emission lines and spikes from the fit, and also Gaussian representation of the emission lines. The reported error bars are the formal fitting errors, coming from the covariant matrix and do not include systematics due to, say, degeneracies.

3.2 Single stellar population analysis

The SSP characteristics are strongly influenced by the last epoch of star formation, and are often considered to be light-weighted averaged characteristics. However, this simplification should be carefully handled (see Trager et al. 2000; Walcher et al. 2006; Trager & Somerville 2009).

First, we determined the SSP-equivalent characteristics using the wavelength range allowed by the models and excluding the emission lines with the iterative, automatic clipping included in ULYSS. Except for IC 745 (low S/N), the quality of the fits is globally satisfactory. In the second experiment, we included the Balmer lines (Hα to Hδ) as independent Gaussian lines in the model (i.e. they are fitted together with the other parameters). The results are similar, but the ages are slightly younger. While the automatic clipping succeeded to mask the core of the lines, their fit, however, also permitted to disentangle the stellar population from the gaseous emission in their wings, so that the solution converged to a younger age to account for deeper Balmer lines.

The latter results are presented in Table 2 and Fig. 1. The ages range from 1 to 2 Gyr and the metallicities from -1.3 dex to Solar for most galaxies. UGC 4599 is essentially an old system ($\approx$9 Gyr). The older and lower metallicity solution found for IC 745 should be taken with caution as the quality of the fit is not satisfactory.

A detailed examination of all the residuals of the fit reveals noticeable misfits in the blue part of the spectra. In particular, the Ca 4227 Å line and to a lesser extent the *G* band are deeper in the best-fitting models than in the observations. These misfits may be an indication that the populations are composite (i.e. not SSPs). The metallic lines of the older stars are diluted by the almost featureless continuum of the blue young stars, and the SSP solution is only a best compromise. Alternatively, the dilution may be due to a nebular continuum associated with the emission. However, this latter contribution is unlikely to be important because the nebular lines themselves are moderate. We nevertheless tested the two possibilities by fitting either composite populations or an SSP plus a featureless continuum. Both types of fits represent improvements of comparable quality, so that we cannot formally choose one or the other hypothesis. Only the presence of the He I 4471 Å (and 4922 Å) lines in absorption in some galaxies (in particular IC 745) is a marginal indication of the composite nature of the populations because those lines are the strongest in B stars.

Since fits with composite populations represent significant improvements and are physically expected, we will now attempt to decompose the populations in multiple components, and therefore reconstruct the history of the star formation.

3.3 Star formation history

In order to derive the SFH, we fitted the spectra starting from a combination of three SSP models. The ages, metallicities, Gaussian parameters of the line-of-sight velocity distribution (redshift and velocity dispersion) and the relative weights of each of these three components are free parameters. A free multiplicative polynomial of the order of 30 was also included in the fitted model. The old population was constrained to an age of 12 Gyr. The age of the young one is bounded in the range $0.1 < \text{age} < 0.6$ Gyr, while the intermediate burst is constrained to have ages between 0.6 and 5 Gyr. The metallicities of the three bursts are free within the limits of the models. The final SFH was obtained by iteratively decreasing the number of components until none of the ages were touching the preset limits and all of the SSPs had positive, significant weights. This initial number of components was proven to be the optimum for SDSS spectra (Tojeiro et al. 2009) and it is also based on our previous experience with similar quality data. Increasing the time resolution, and therefore the number of free parameters, also increases the degeneracies between the components and the χ^2-space become complex with multiple local minima. Other programs, like STECKMAP (Ocvirk et al. 2006) or STARLIGHT (Cid Fernandes et al. 2005), decompose the population on to a finer grained grid, but apply a regularization that also reduces the time resolution. Using better quality data would help, but expanding the wavelength coverage would be the best solution to reduce the degeneracies.

We also included the emission lines in the fitted models, similarly to what was done in the previous section. However, we did not include any additive term. The results are presented in Figs 2, 3 and Table 3. The quality of the fits can be visually inspected in Appendix A. As we do not have a handle on the real SFR within the boxes we assume them to be constant (Fig. 2). We compute the limits of these bins as the middle (in logarithm) of the derived SSP ages. The integral of the SFR over the full time gives the stellar mass of the galaxies within the 3-arcsec fibre of SDSS.

The SFHs reconstructed with Pegase-HR/Elodie 3.2 and with Vazdekis/Miles are consistent, and the second is more precise

[5] http://www.iac.es/galeria/vazdekis/vazdekis_models_ssp_seds.html
[6] http://www2.iap.fr/pegase/pegasehr/

Table 2. SSP-equivalent ages and metallicities of our sample when the emission lines (from Hα to Hδ) are fitted simultaneously with the other parameters.

	Pegase-HR/Elodie 3.2		Vazdekis/Miles	
Name	Age (Myr)	[Fe/H]	Age (Myr)	[Fe/H]
NGC 4286	1301 ± 101	−0.15 ± 0.06	2035 ± 149	−0.50 ± 0.05
NGC 3265	1711 ± 83	−0.71 ± 0.02	1400 ± 26	−0.84 ± 0.02
NGC 3353	1069 ± 26	−0.79 ± 0.03	1188 ± 23	−1.19 ± 0.02
NGC 3928	1650 ± 51	−0.17 ± 0.03	1484 ± 45	−0.13 ± 0.02
IC 0745	5395 ± 255	−1.83 ± 0.04	1197 ± 23	−1.66 ± 0.02
NGC 4323	3021 ± 847	−0.70 ± 0.08	4074 ± 983	−0.70 ± 0.06
VCC 797	2344 ± 396	−0.66 ± 0.10	3976 ± 1077	−0.71 ± 0.06
VCC 1949	2676 ± 261	−0.15 ± 0.07	3943 ± 726	−0.00 ± 0.03
IC 3025	1191 ± 56	−0.61 ± 0.08	1755 ± 133	−1.18 ± 0.05
VCC 1993	2290 ± 139	−0.18 ± 0.06	2161 ± 161	−0.26 ± 0.06
UGC 04599	8527 ± 549	−0.35 ± 0.03	6474 ± 474	−0.23 ± 0.02
Mrk 0706	1654 ± 75	−1.03 ± 0.04	1715 ± 59	−1.09 ± 0.03
SDSS J0936	1917 ± 123	−0.88 ± 0.07	1890 ± 163	−1.19 ± 0.06
IC 0676	1416 ± 29	−0.69 ± 0.03	1355 ± 17	−0.77 ± 0.02
IC 0692	1542 ± 96	−1.21 ± 0.05	1040 ± 121	−1.18 ± 0.03
IC 0719	4372 ± 503	0.02 ± 0.02	4265 ± 511	0.06 ± 0.02
UGC 06655	1610 ± 109	−1.03 ± 0.03	1484 ± 40	−1.13 ± 0.03
2MASX J1146	1779 ± 82	−0.95 ± 0.03	2829 ± 433	−1.23 ± 0.03
NGC 5338	744 ± 23	−0.47 ± 0.03	765 ± 15	−0.33 ± 0.02
dE, 1R_e	7037 ± 2187	−0.61 ± 0.09	5530 ± 1141	−0.54 ± 0.09
dE, 1 arcsec	3159 ± 580	−0.32 ± 0.07	2840 ± 853	−0.34 ± 0.07
TTD	1315 ± 48	−0.85 ± 0.10	1247 ± 77	−0.69 ± 0.12
TTD+1	6758 ± 2621	−0.78 ± 0.19	4464 ± 2360	−0.64 ± 0.20

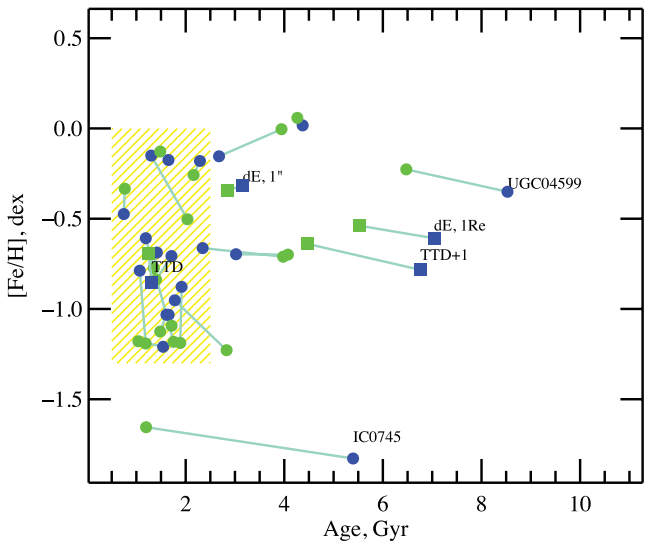

Figure 1. SSP-equivalent metallicity versus age (see also Table 2). The hashed yellow region marks the typical area occupied by our TTDs. The blue symbols are from the analysis with Pegase-HR/Elodie 3.2 and the green symbols are those from Vazdekis/Miles. We plot the individual galaxies with circles, while the stacked spectra (see Section 4.2.2) are presented with squares and are annotated. The outliers are also marked.

(e.g. giving results with smaller error bars). We repeated the Vazdekis/Miles analysis restricting to the wavelength range of the Pegase-HR/Elodie 3.2 models. This time the parameters derived using the two models were with similar error bars. Hence, the precision gain is due to the extended (towards the red) wavelength range.

Most of the objects are consistent with a constant SFR. A purely old population would not be distinguished from a rapidly exponentially declining SFR, and multiple burst would be smeared out, but our analysis restores the mean SFR during the main large era of the evolution.

The only clear deviation from constant SFR is IC 745, which is characterized by a dominant old population and a significant young burst, but lack of an intermediate-age population. Almost all H I-detected galaxies outside of Virgo show a relatively strong, recent burst.

In average, all galaxies show a strong metal enrichment (about 1 dex) after their first star formation episode, which is followed by a milder increase in their youngest stellar population (Fig. 3). For some galaxies it may seem that the metallicity decreases with time; however, these metallicities are often associated with large error bars ($\gtrsim$1 dex).

3.4 Evidence for composite populations

The SSP fit with an additional hot continuum provides a good representation of the spectra. However, a careful visual comparison of the residuals may however provide evidence for the presence of a young population besides the obvious presence of strong emission Balmer lines. The He I absorption lines, in particular the ones at 4471 and 4922 Å, are characteristic features of B stars. (The He lines peak at a few 10^7 yr in SSPs; González Delgado et al. 2005.) However, as for the Balmer lines, they are likely filled with emission. In some galaxies (NGC 3353, UGC 6655) both lines appear in emission, while for others (NGC 3065, Mrk 0706) only He I 4471 is visible in the residual emissions. In IC 745, the lines are seen in absorption in the residuals of the fit to an SSP plus power law and in emission in the residuals of the SFH fit. The appearance of these lines in absorption in the SSP plus power-law fit indicates that the SSP fit is insufficient and that a young population must be present.

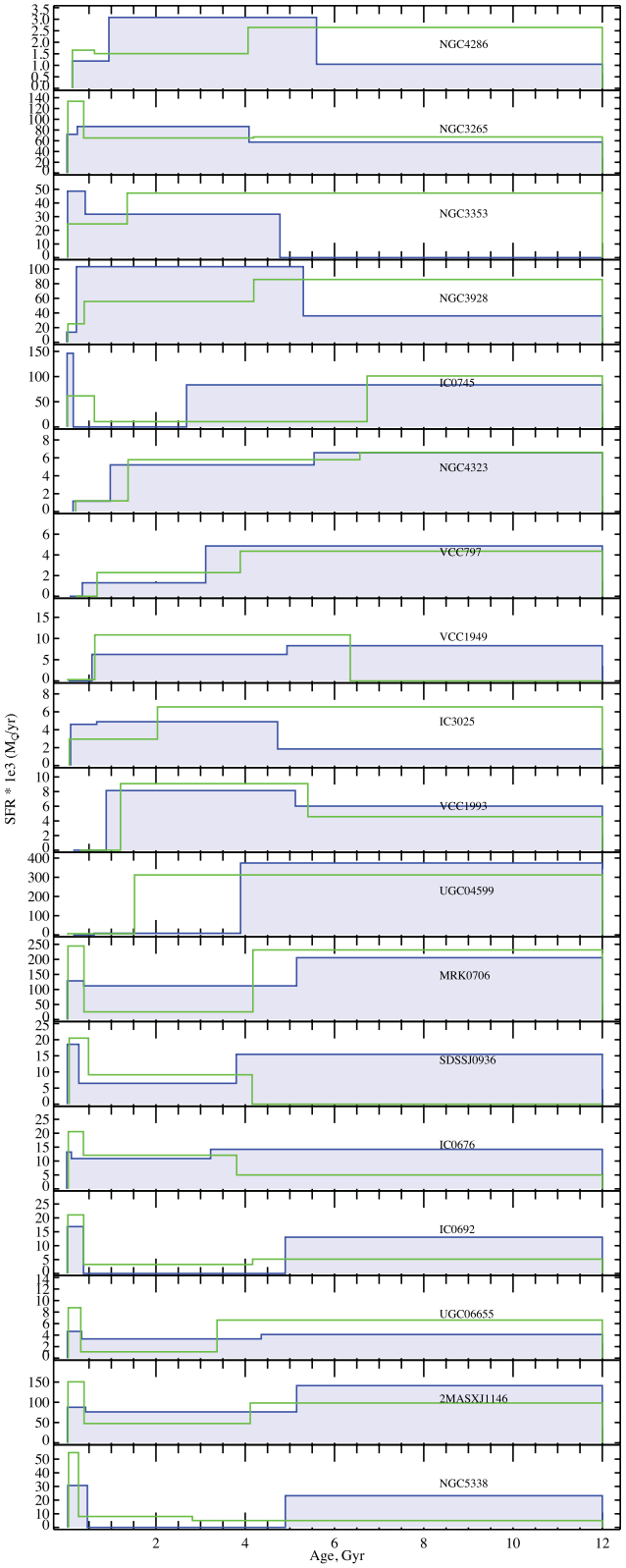

Figure 2. SFHs of our sample of galaxies, reconstructed with Pegase-HR/Elodie 3.2 (blue) and Vazdekis/Miles (green) stellar population models. Each panel represents the SFR as a function of the look-back time.

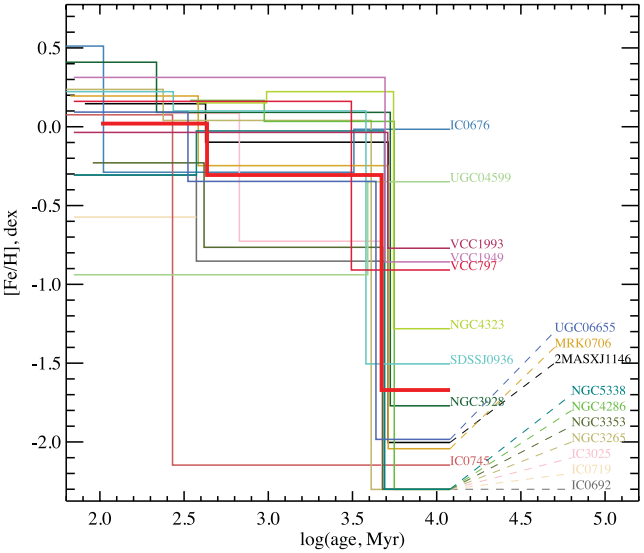

Figure 3. Metallicity evolution as a function of age for our sample. Different colours correspond to different galaxies according to the legend. The thick red line represents the averaged metallicity evolution. We plot the results from the inversion with Pegase-HR/Elodie 3.2 models.

4 DISCUSSION

4.1 Environment

Environmental influences on dwarf galaxies manifest themselves most strongly through the morphology–density relation – early-type galaxies live in high-density environments, while late-type galaxies are found in low-density environments (Einasto et al. 1974; van den Bergh 1994; Bouchard et al. 2009). In a dense environment, ram-pressure stripping (Einasto et al. 1974; Boselli et al. 2008) and/or tidal effects (Moore, Lake & Katz 1998; Mayer et al. 2006) can remove the ISM from dwarf galaxies, halting the star formation and transforming them from late to early types.

Several observational studies find that, indeed, in dense environments (like Virgo or Fornax clusters) just a handful of dwarfs are detected in H I (e.g. Conselice et al. 2003 and references therein), Hα (e.g. Drinkwater et al. 2001) or infrared dust emission (e.g. de Looze et al. 2010). Most of the dwarfs with a detected ISM lie in the outskirts of the cluster environment. Similar behaviour is observed for fainter early-type dwarfs (like dSphs) in groups, including the Local Group (Einasto et al. 1974; van den Bergh 1994; Bouchard, Carignan & Staveley-Smith 2006; Bouchard et al. 2009). However, it is worth mentioning that due to observational limitations (e.g. contamination along the line of sight, indirect measurements and ambiguous transformation factors) some fraction of the ISM may be missed. For example, VCC 390, the only galaxy of the Virgo subsample located in the central region of the cluster, is suspected to be a false detection due to the contamination in the telescope lobe (thus, we exclude it from the selection).

Although the environmental influence is relevant to our studies (hence our last columns in Table 1), our sample is neither complete (e.g. we do not cover the full Virgo survey) nor homogeneous (we have galaxies situated in environments with different densities, see Table 1), we therefore restrain ourselves from further analysis. Nevertheless, we searched for differences in the SFH associated with the isolation of the galaxies (see Section 2.1). We did not observe any connection, either because there is none or possibly because of the sample. Again, we note that an environmental dependence of the

Table 3. Population histories of the TTDs, reconstructed with three episodes of star formation and Pegase-HR/Elodie 3.2 synthesis models. The first column is the name of the galaxy, followed by the age, metallicity and light fraction for the young (from 0–0.6 Gyr), intermediate (from 0.6 to 5 Gyr) and old (∼12 Gyr) populations.

	Young			Inter			Old	
Name	Age (Gyr)	[Fe/H] (dex)	Fraction (per cent)	Age (Gyr)	[Fe/H] (dex)	Fraction (per cent)	Age (Gyr)	[Fe/H] (dex)	Fraction (per cent)
2MASX J1146	0.08 ± 0.01	0.15 ± 0.10	37	2.21 ± 0.60	−0.10 ± 0.25	25	12.00 (fixed)	−2.00 ± 0.15	37
IC 0676	0.01 ± 0.00	0.51 ± 0.12	29	0.87 ± 0.14	−0.29 ± 0.13	55	12.00 (fixed)	−0.02 ± 0.22	15
UGC 04599	–	–	–	1.26 ± 1.12	−0.94 ± 0.97	8	12.00 (fixed)	−0.35 ± 0.05	91
VCC 1949	–	–	–	2.03 ± 0.79	0.31 ± 0.23	50	12.00 (fixed)	−0.86 ± 0.17	49
SDSS J0936	0.06 ± 0.02	0.22 ± 0.19	43	1.20 ± 0.62	0.10 ± 0.32	22	12.00 (fixed)	−1.50 ± 0.48	34
NGC 3928	0.02 ± 0.00	0.41 ± 0.20	13	2.34 ± 0.18	0.09 ± 0.05	66	12.00 (fixed)	−1.77 ± 0.11	19
Mrk 0706	0.07 ± 0.01	0.20 ± 0.08	37	2.21 ± 0.36	−0.25 ± 0.23	26	12.00 (fixed)	−2.04 ± 0.12	36
UGC 06655	0.07 ± 0.01	0.09 ± 0.13	37	1.58 ± 0.24	−0.35 ± 0.14	36	12.00 (fixed)	−1.98 ± 0.15	26
NGC 3353	0.09 ± 0.01	−0.23 ± 0.05	55	1.90 ± 0.18	−0.77 ± 0.07	44	–	–	–
NGC 3265	0.04 ± 0.01	0.24 ± 0.09	32	1.39 ± 0.19	0.04 ± 0.06	45	12.00 (fixed)	−2.30 ± -0.00	22
NGC 4286	0.34 ± 0.23	0.17 ± 0.47	25	2.61 ± 0.66	0.03 ± 0.16	56	12.00 (fixed)	−2.30 ± 0.00	18
IC 0745	0.04 ± 0.00	0.08 ± 0.03	53	–	–	–	12.00 (fixed)	−2.15 ± 0.03	46
IC 0692	0.07 ± 0.00	−0.31 ± 0.05	75	–	–	–	12.00 (fixed)	−0.85 ± 0.09	25
VCC 797	–	–	–	0.81 ± 0.69	0.16 ± 0.58	33	12.00 (fixed)	−0.91 ± 0.14	66
IC 3025	0.24 ± 0.19	0.08 ± 0.40	31	1.86 ± 0.92	−0.73 ± 0.15	56	12.00 (fixed)	−2.30 ± 0.00	12
VCC 1993	–	–	–	2.19 ± 1.08	−0.04 ± 0.27	67	12.00 (fixed)	−0.77 ± 0.35	32
NGC 5338	0.11 ± 0.01	−0.31 ± 0.04	84	–	–	–	12.00 (fixed)	−0.03 ± 0.12	16
NGC 4323	0.37 ± 0.73	0.15 ± 1.40	11	2.56 ± 1.87	0.22 ± 0.42	39	12.00 (fixed)	−1.28 ± 0.58	48

Figure 4. Luminosity–metallicity relation for our TTDs and the dEs from Koleva et al. (2009a). The former are plotted with blue stars and the latter with red circles. With grey circles we plot galaxies from Koleva et al. (2011, and references therein).

gas content and positioning within the cluster/group was observed in other studies (e.g. Conselice et al. 2003; Bouchard et al. 2009).

4.2 Comparison with diffuse elliptical galaxies

The purpose of this study is to determine whether the TTDs can evolve into classical dEs. Therefore, we will first investigate if both types of dwarfs occupy the same area in the luminosity–metallicity plane, and secondly, if their SFHs are similar. We will also follow the evolution of a 'passively fading' TTD.

4.2.1 Metallicity–luminosity relations

A galaxy's metallicity reflects its evolutionary stage, or how much of its initial gas was processed in stars, and to what extent the metals were kept by the galaxy. Feedback, or the energy released by supernovae and stellar winds, regulates the star formation by heating the gas and releasing the newly formed metals into the ISM. It is capable of venting metals from dwarf galaxies, where the gravitational potentials can be overcome by energetic winds, thus depleting the galaxy of metals. The quantity of metals released from the galaxy will depend on the galactic geometry, mass, density and star formation strength. Thus, comparing metallicities of galaxies with similar mass/luminosities we can access to what extent they had similar SFHs, masses and geometries in the past.

To probe if the star formation proceeds in a similar fashion in TTDs and dEs, we will first look at the luminosity–metallicity relation (e.g. Tremonti et al. 2004). To set a base for the comparison we use data from Koleva et al. (2011) for early-type galaxies (dSph, dE, TTDs, E, S0) spanning a luminosity range of 14 mag, Fig. 4.

By construction, our sample of TTDs has similar optical magnitudes as the dEs from Koleva et al. (2009a). Now, we will compare their metallicities. Since the TTDs have extended until present SFHs, we will not use the SSP-equivalent parameters, but luminosity-weighted metallicities from the intermediate and old population (Table 3). Hence, we compare the same stellar populations of dEs and TTDs. The results are displayed in Fig. 4. Both

families of galaxies occupy the same region on the diagram. This is not unexpected since while a population ages its luminosity decreases, but so does the luminosity-weighted metallicity, which is not anymore governed by the youngest, brightest, most metal-rich stars. This effect is clearly seen in Fig. 1, where the aged TTDs occupy the same region as the dE galaxies. Hence, the star formation and the feedback must have been similar in these two types of objects (as we will confirm in the next section). As a word of caution, we note that the relation seems to be flatter for our TTDs than for the sample of dEs. This may be an artefact from the difference between SSP-equivalent and luminosity-weighted metallicities (see Trager et al. 2000) and/or the limited range in magnitudes.

4.2.2 Star formation histories

We will now compare the SFHs of both classes of galaxies, and, as the SFH shown in Fig. 2 presents a fair homogeneity, we will stack the TTDs' spectra.

To increase the S/N and to smooth the peculiarities, we stacked the spectra of the TTDs located in the yellow region of Fig. 1. The 'old' TTD (UGC 4599) was not included, nor IC 745 which is atypical. Prior to the co-adding of the spectra, we subtracted the Balmer emission lines since their broadening varies from spectrum to spectrum in a manner loosely correlated with the velocity dispersion. We weighted the spectra by the square of the S/N in order to optimize the resulting S/N, and excluded the spectral regions rejected during the composite population fit (Section 3). The stacked spectrum has S/N ~ 80.

For the comparison between the SFHs of TTDs and dEs we used the dEs from Koleva et al. (2009a). The spectra of the dEs were stacked as follows: first we excluded all galaxies with emission lines (which in the context of this work will be classified as TTDs), secondly we convolved the spectra to a common velocity dispersion of 100 km s^{-1}and finally we normalized them to 1, using a polynomial of third degree. We stacked the spectra both in the central 1 arcsec and 1 R_e extractions.

For all the stacked spectra we performed composite SSP analyses, fixing the age limits of the bursts as $t_{young} \in [80, 600]$, $t_{intermediate} \in [600, 5000]$ and $t_{old} = 12\,000$ Myr. The other fitting parameters are the same as in Section 3.3. The Pegase-HR/Elodie 3.2 and Vazdekis/Miles determinations are consistent. The results are plotted in Fig. 5.

Our TTDs obviously contain more young stars (as clearly seen from the recent peak in the SFR, Fig. 5), so to make a meaningful comparison we take the SFH, suppose a sudden quenching of the star formation and let the modelled population age by 1, 2 or 3 Gyr. The result of the analysis with a composite SSP model 'passively evolved' for 1 Gyr is presented in the middle panel of Fig. 5. We compare thus obtained SFHs with the SFHs of the central 1 arcsec and 1 R_e of the dEs. The mean SFH of the TTDs differs from the dEs only in the last 0.5–1 Gyr. However, after 1 Gyr of a passive evolution this difference disappears. Both families of galaxies indicate strong star formation in the beginning which declines at about 5 and 6 Gyr ago. Obviously, we do not have the resolution of the colour–magnitude diagram analyses of the Local Group dwarf galaxies, and we cannot distinguish details in the SFHs, but the overall shape of the stellar production history is very similar. In addition, they occupy the same metallicity–luminosity relation, which in turn indicates similar feedback and metal enrichment. Hence, we conclude that there were no major discrepancies in the details of their past star formation and a 'passively evolving' TTD would be identical to a dE.

4.3 Evolutionary connection

Given the similarities between TTDs and dEs we found, we naturally search for mechanisms related to dE formation and evolution that would produce TTDs. dEs are predominantly segregated in densely populated vicinity (Binggeli, Sandage & Tammann 1988). Moreover, simulations of dwarfs (e.g. Valcke et al. 2008) with total masses $>10^8$ M$_\odot$ have shown that their supernovae are not capable of sweeping away their full gas reservoir. Hence, external mechanisms must play a major role in shaping dEs we observe today. Since dEs are strongly affected by environment, TTD producing mechanisms are likely to be also environmentally linked. In the previous subsection, we established that the SFHs and the SSP-equivalent metallicities (for a given mean mass) are identical between the dEs and the TTDs and that a passively evolving TTD will turn into a galaxy with the same stellar population as a dE.

In this section, we intend to place the TTDs in a broader picture of dwarf evolution. Based on our results and the literature data, we propose the following evolutionary scenario. If a star-forming galaxy (BCD or dIrr) with stellar mass around 10^9 M$_\odot$ does not enter into a dense environment (cluster or group), it will keep its gas reservoir as the feedback from the supernovae is not capable to fully overcome the gravitational potential (as shown by simulations of dwarfs; Valcke et al. 2008). However, theory (Valcke et al. 2008; Revaz et al. 2009; Stinson et al. 2009; Schroyen et al. 2011) and observations (van Zee 2002) suggest that a non-rotating dwarf galaxy (BCD-like) will have an episodic, bursty star formation. Such a galaxy will have quiescent phases where it may be observed as a TTD (no star formation but gas abundant). Sánchez Almeida et al. (2009) analysed the stacked SDSS spectra of such QBCDs and concluded that they have metallicities similar to active BCDs. These types of TTDs should be observed in scarcely populated environment and, according to observational results (Koleva et al. 2009a) and simulations (Schroyen et al. 2011), should have steep metallicity gradients.

The second way to produce a TTD could be when a star-forming dwarf falls into a dense environment. If the galaxy is lucky enough and stays on a tangential orbit, away from the dense centre, it will keep some of its star formation and/or gas (the ram-pressure stripping will be still active at large galocentral radius) and be classified as a TTD. Indeed, most of the galaxies with gas and/or star formation are observed in the peripheries of the cluster and groups (Einasto et al. 1974; van den Bergh 1994; Conselice et al. 2003; Bouchard et al. 2006, 2009). We propose that this intermediate situation will continue until the galaxy changes its orbit and enters in more violent environment, or until the remaining gas is consumed. If this galaxy is observed in its quiescent phase, but observations failed to detect its gas reservoir (because of a too shallow survey or/and not targeting the right gas temperature) the galaxy will be a false dE. De Rijcke, Van Hese & Buyle (2010) found that less than 30 per cent of the dwarf population of Fornax cluster is on tangential orbits. Indeed, Drinkwater et al. (2001), based on Hα observations, concluded that about the same fraction of dwarfs in Fornax are star forming. Thus, the relatively small population of TTDs in clusters can be explained with the lower probability of tangential orbits. If a star-forming galaxy enters on to a radial orbit, its gas is going to be stripped almost instantaneously (for less than 100 Myr; Boselli et al. 2008) and the chances to observe such a TTD will be extremely low. Hence, we can extrapolate that if a star-forming dwarf enters a

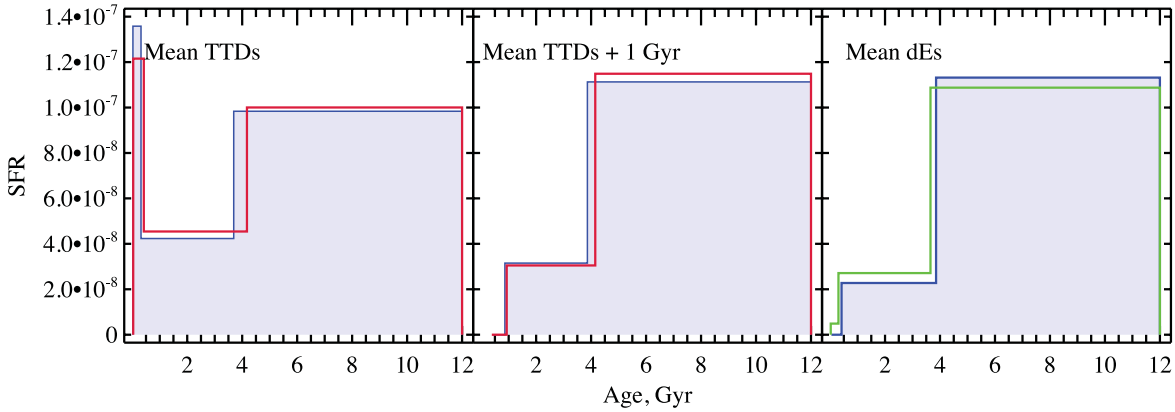

Figure 5. Comparison of the SFH of dEs and TTDs. With blue we plot the analyses with Pegase-HR/Elodie models, while with red we plot the results from Vazdekis/Miles fits. In the first two panels we plot the TTDs (now and after 1 Gyr of passive evolution, left and middle, respectively), while in the last the stacked dE SFHs for central arcsec extraction (in green) and the one effective radius extraction (in blue), both analysed with Pegase-HR/Elodie 3.2. The SFRs were obtained by normalizing the mass to 1 $M_{\odot}$ for each of the stacks.

cluster in a radial orbit it will be almost instantly transformed into a dE, without passing through the TTD phase.

To summarize there must be two types of TTDs. The first one corresponds to a low-activity phase of a BCD (between two bursts of star formation). The second one consists of star-forming dwarfs captured by a cluster potential in a tangential orbit and on its way of becoming a dE. Our stellar population analyses cannot distinguish the two types of objects.

5 CONCLUSION

We chose a sample of local galaxies ($cz < 3000$ km s^{-1}) classified in the literature as TTDs. Our galaxies were selected to be faint ($-19 < M_B < -14$ mag) and have SDSS spectra. We analysed their stellar population parameters (SSP-equivalent ages and metallicities, SFHs) using a full spectrum fitting technique with ULYSS. We compared thus derived population parameters with the same quantities of dE galaxies. We found the following.

(i) TTDs have relatively young SSP-equivalent ages – between ∼1 and 2 Gyr old.

(ii) The TTDs occupy the same region on the luminosity–metallicity relation as dEs (when their old and intermediate stellar populations are considered).

(iii) Their SFHs are characterized by a roughly constant SFR until present.

(iv) Their metal-enrichment history is consistent with a rapid enrichment after the first star formation episode and milder enrichment afterwards.

(v) After a few Gyr of passive evolution the TTDs have similar SFHs to the dEs.

We conclude that a passively evolving TTD will be indistinguishable from a dE, at least for what concerns its stellar population.

We suggest two possible origins for the TTDs; they may be BCDs in a low-activity phase resulting from internal processes. During a starburst the gas is heated and while it is cooling down the star formation is reduced or suspended; this may happen cyclically. Others may be star-forming galaxies on tangential orbits, which are on their way to become dEs. It may be difficult to determine the exact nature of a given TTD. The effects of the environment and the morphology of the dwarf's gas reservoir, possibly distorted by ram pressure, may hold the keys to their evolution.

ACKNOWLEDGMENTS

MK is a postdoctoral fellow of the Fund for Scientific Research- Flanders, Belgium (FWO11/PDO/147) and Marie Curie (Grant PIEF-GA-2010-271780). We thank the referee, J. Sánchez Almeida, for his comments, which helped improving the content and clarifying the paper. We thank J. Schroyen for the critical reading and useful comments and D. Makarov for our discussions on the environment. We acknowledge the use of SDSS DR7 (the full acknowledgment can be found at http://www.sdss.org/collaboration/credits.html) and HyperLeda (http://leda.univ-lyon1.fr) data bases.

REFERENCES

Abazajian K. (for the Sloan Digital Sky Survey), 2009, ApJS, 182, 543
Asari N. V., Cid Fernandes R., Stasińska G., Torres-Papaqui J. P., Mateus A., Sodré L., Schoenell W., Gomes J. M., 2007, MNRAS, 381, 263
Beaulieu S. F., Freeman K. C., Carignan C., Lockman F. J., Jerjen H., 2006, AJ, 131, 325
Binggeli B., Sandage A., Tammann G. A., 1988, ARA&A, 26, 509
Boselli A., Boissier S., Cortese L., Gavazzi G., 2008, ApJ, 674, 742
Bouchard A., Jerjen H., Da Costa G. S., Ott J., 2005, AJ, 130, 2058
Bouchard A., Carignan C., Staveley-Smith L., 2006, AJ, 131, 2913
Bouchard A., Da Costa G. S., Jerjen H., 2009, AJ, 137, 3038
Bouchard A., Prugniel P., Koleva M., Sharina M., 2010, A&A, 513, A54
Buyle P., De Rijcke S., Michielsen D., Baes M., Dejonghe H., 2005, MNRAS, 360, 853
Cid Fernandes R., Mateus A., Sodré L., Stasińska G., Gomes J. M., 2005, MNRAS, 358, 363
Cloet-Osselaer A., De Rijcke S., Schroyen J., Dury V., 2012, MNRAS, 423, 735
Conselice C. J., O'Neil K., Gallagher J. S., Wyse R. F. G., 2003, ApJ, 591, 167
Dalcanton J. J. et al., 2009, ApJS, 183, 67
Davidge T. J., 2003, ApJ, 597, 289
de Looze I. et al., 2010, A&A, 518, L54
De Rijcke S., Zeilinger W. W., Dejonghe H., Hau G. K. T., 2003, MNRAS, 339, 225
De Rijcke S., Van Hese E., Buyle P., 2010, ApJ, 724, L171
Dellenbusch K. E., Gallagher J. S. III, Knezek P. M., 2007, ApJ, 655, L29
Dellenbusch K. E., Gallagher J. S. III, Knezek P. M., Noble A. G., 2008, AJ, 135, 326
di Serego Alighieri S. et al., 2007, A&A, 474, 851

Drinkwater M. J., Gregg M. D., Holman B. A., Brown M. J. I., 2001, MNRAS, 326, 1076
Einasto J., Saar E., Kaasik A., Chernin A. D., 1974, Nat, 252, 111
González Delgado R. M., Cerviño M., Martins L. P., Leitherer C., Hauschildt P. H., 2005, MNRAS, 357, 945
Goto T., Yamauchi C., Fujita Y., Okamura S., Sekiguchi M., Smail I., Bernardi M., Gomez P. L., 2003, MNRAS, 346, 601
Grebel E. K., Gallagher J. S. III, Harbeck D., 2003, AJ, 125, 1926
Grossi M., Disney M. J., Pritzl B. J., Knezek P. M., Gallagher J. S., Minchin R. F., Freeman K. C., 2007, MNRAS, 374, 107
Grossi M. et al., 2009, A&A, 498, 407
Hidalgo S. L., Aparicio A., Martínez-Delgado D., Gallart C., 2009, ApJ, 705, 704
Hidalgo S. L. et al., 2011, ApJ, 730, 14
Knezek P. M., Sembach K. R., Gallagher J. S. III, 1999, ApJ, 514, 119
Koleva M., Prugniel P., Ocvirk P., Le Borgne D., Soubiran C., 2008, MNRAS, 385, 1998
Koleva M., de Rijcke S., Prugniel P., Zeilinger W. W., Michielsen D., 2009a, MNRAS, 396, 2133
Koleva M., Prugniel P., Bouchard A., Wu Y., 2009b, A&A, 501, 1269
Koleva M., Prugniel P., de Rijcke S., Zeilinger W. W., 2011, MNRAS, 417, 1643
Le Borgne D., Rocca-Volmerange B., Prugniel P., Lançon A., Fioc M., Soubiran C., 2004, A&A, 425, 881
Lisker T., Glatt K., Westera P., Grebel E. K., 2006, AJ, 132, 2432
Mathis H., Charlot S., Brinchmann J., 2006, MNRAS, 365, 385
Mayer L., Mastropietro C., Wadsley J., Stadel J., Moore B., 2006, MNRAS, 369, 1021
Michielsen D., de Rijcke S., Zeilinger W. W., Prugniel P., Dejonghe H., Roberts S., 2004, MNRAS, 353, 1293
Moore B., Lake G., Katz N., 1998, ApJ, 495, 139
Ocvirk P., Pichon C., Lançon A., Thiébaut E., 2006, MNRAS, 365, 74
Paturel G., Petit C., Prugniel P., Theureau G., Rousseau J., Brouty M., Dubois P., Cambrésy L., 2003, A&A, 412, 45
Prugniel P., Simien F., 1996, A&A, 309, 749
Prugniel P., Soubiran C., 2001, A&A, 369, 1048
Prugniel P., Golev V., Maubon G., 1999, A&A, 346, L25
Revaz Y. et al., 2009, A&A, 501, 189
Sánchez Almeida J., Aguerri J. A. L., Muñoz-Tuñón C., Vazdekis A., 2009, ApJ, 698, 1497
Sánchez-Blázquez P. et al., 2006, MNRAS, 371, 703
Sandage A., Binggeli B., 1984, AJ, 89, 919
Sandage A., Fomalont E., 1993, ApJ, 407, 14
Sandage A., Hoffman G. L., 1991, ApJ, 379, L45
Schild R. E., 1977, AJ, 82, 337
Schlegel D. J., Finkbeiner D. P., Davis M., 1998, ApJ, 500, 525
Schroyen J., De Rijcke S., Valcke S., Cloet-Osselaer A., Dejonghe H., 2011, MNRAS, 416, 601
Stinson G. S., Dalcanton J. J., Quinn T., Gogarten S. M., Kaufmann T., Wadsley J., 2009, MNRAS, 395, 1455
Tojeiro R., Wilkins S., Heavens A. F., Panter B., Jimenez R., 2009, ApJS, 185, 1
Trager S. C., Somerville R. S., 2009, MNRAS, 395, 608
Trager S. C., Faber S. M., Worthey G., González J. J., 2000, AJ, 120, 165
Tremonti C. A. et al., 2004, ApJ, 613, 898
Valcke S., de Rijcke S., Dejonghe H., 2008, MNRAS, 389, 1111
van den Bergh S., 1994, ApJ, 428, 617
van Zee L., 2002, in Grebel E. K., Brandner W., eds, ASP Conf. Ser. Vol. 285, Modes of Star Formation and the Origin of Field Populations. Astron. Soc. Pac., San Francisco, p. 333
Vazdekis A., Sánchez-Blázquez P., Falcón-Barroso J., Cenarro A. J., Beasley M. A., Cardiel N., Gorgas J., Peletier R. F., 2010, MNRAS, 404, 1639
Walcher C. J., Böker T., Charlot S., Ho L. C., Rix H.-W., Rossa J., Shields J. C., van der Marel R. P., 2006, ApJ, 649, 692
Weisz D. R. et al., 2011, ApJ, 739, 5
Wu Y., Singh H. P., Prugniel P., Gupta R., Koleva M., 2011, A&A, 525, A71
York D. G. et al., 2000, AJ, 120, 1579

APPENDIX A: FITS OF THE GALAXIES

In this appendix, we present the fits from the multiple population analyses (Section 3.3, Fig. A1), so as to illustrate the quality of the fits and visualize the misfits. For a better representation, the spectra of the galaxies are normalized to one. For a better assessment of the quality of the fit we plot the residuals in a separate panel with an expanded scale (±20 per cent). Our fits are generally satisfactory, limited by the S/N of the data. We do not observe any major misfit at any specific lines, in particular the Mg region is well fitted, which in turn indicates good match of the α-element abundances of these galaxies as compared to the solar neighbourhood. The automatic clipping of the spectrum did not mask any important absorption features and in general the masked region is less than 1 per cent from the original pixel number. The region around 5892 Å (NaD) and 6250 Å is masked in the models as some residual telluric features are almost always present both in the models (based on empirical stellar libraries) and in the observations. In most of the cases the multiplicative polynomial (cyan in Fig. A1) is around 1, indicating good flux calibration and extinction correction.

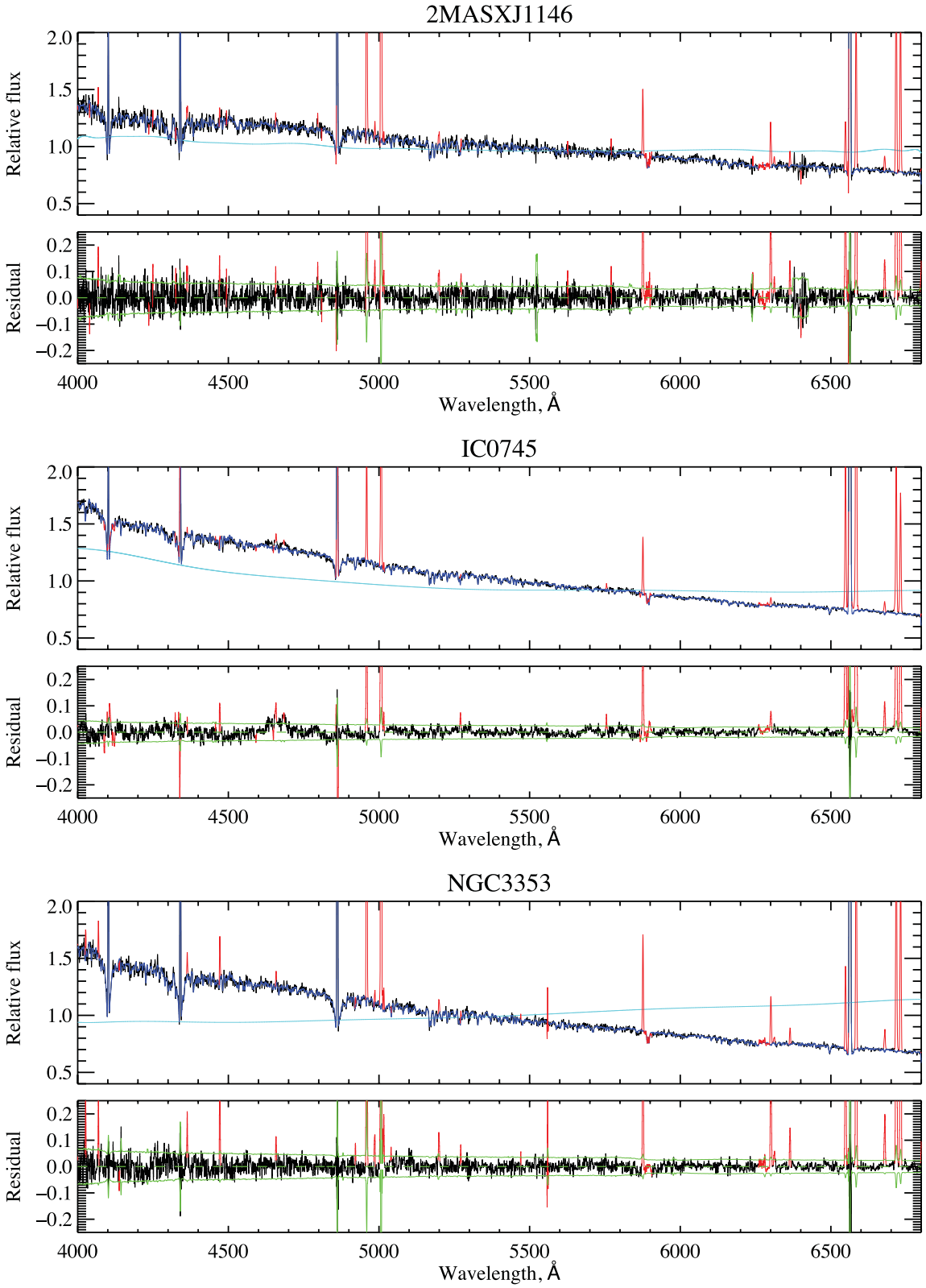

Figure A1. Three component fits to the TTD spectra. Each fit is shown in two panels. In the top panels we plot the SDSS spectrum (with black), the best-fitting model (with blue), the multiplicative continuum (with cyan). In the bottom panel we plot the observation minus model residuals (with black) and 1σ standard deviation of the observations (with green). In both panels the masked pixels are plotted with red.

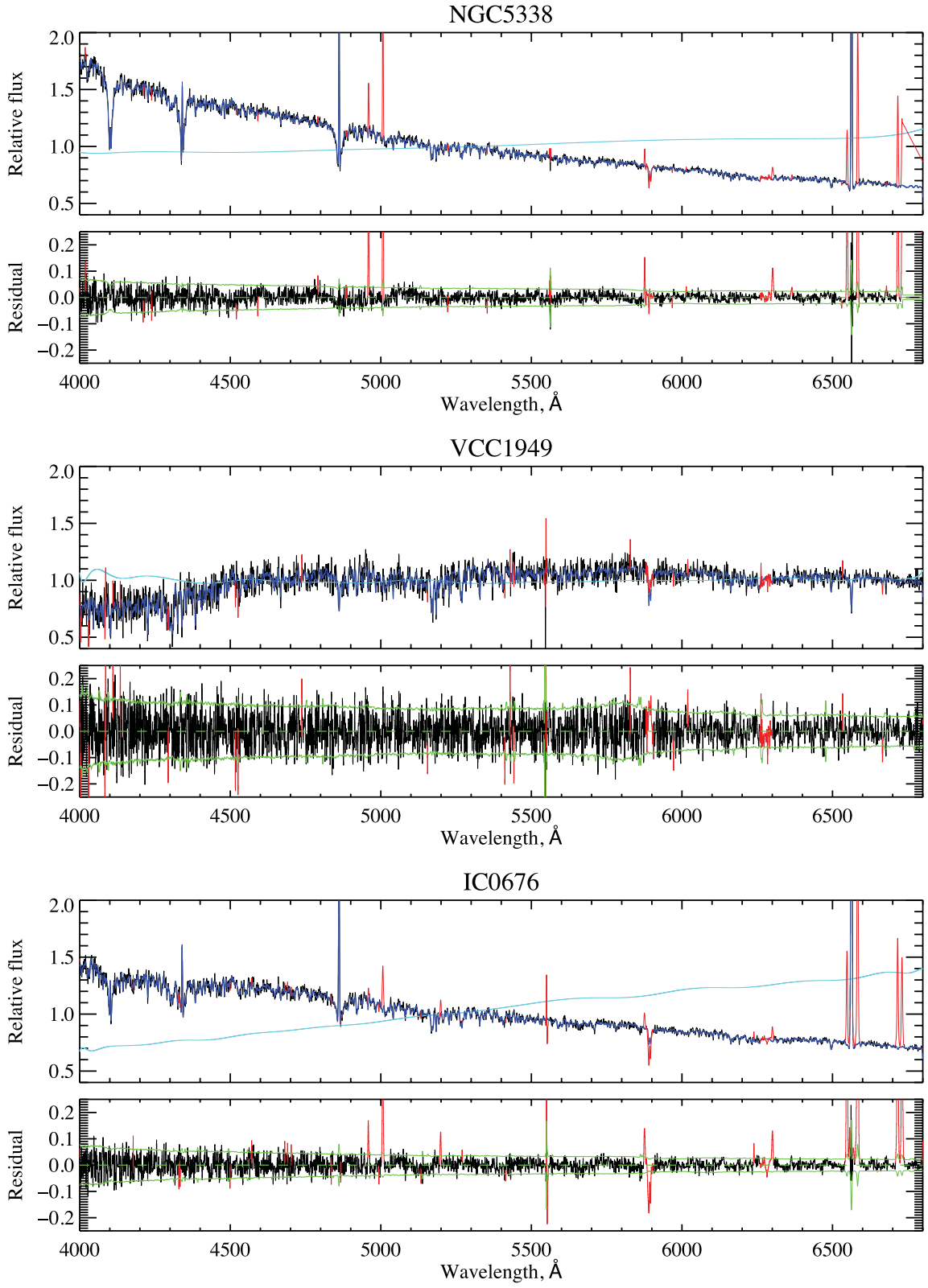

Figure A1 – *continued*

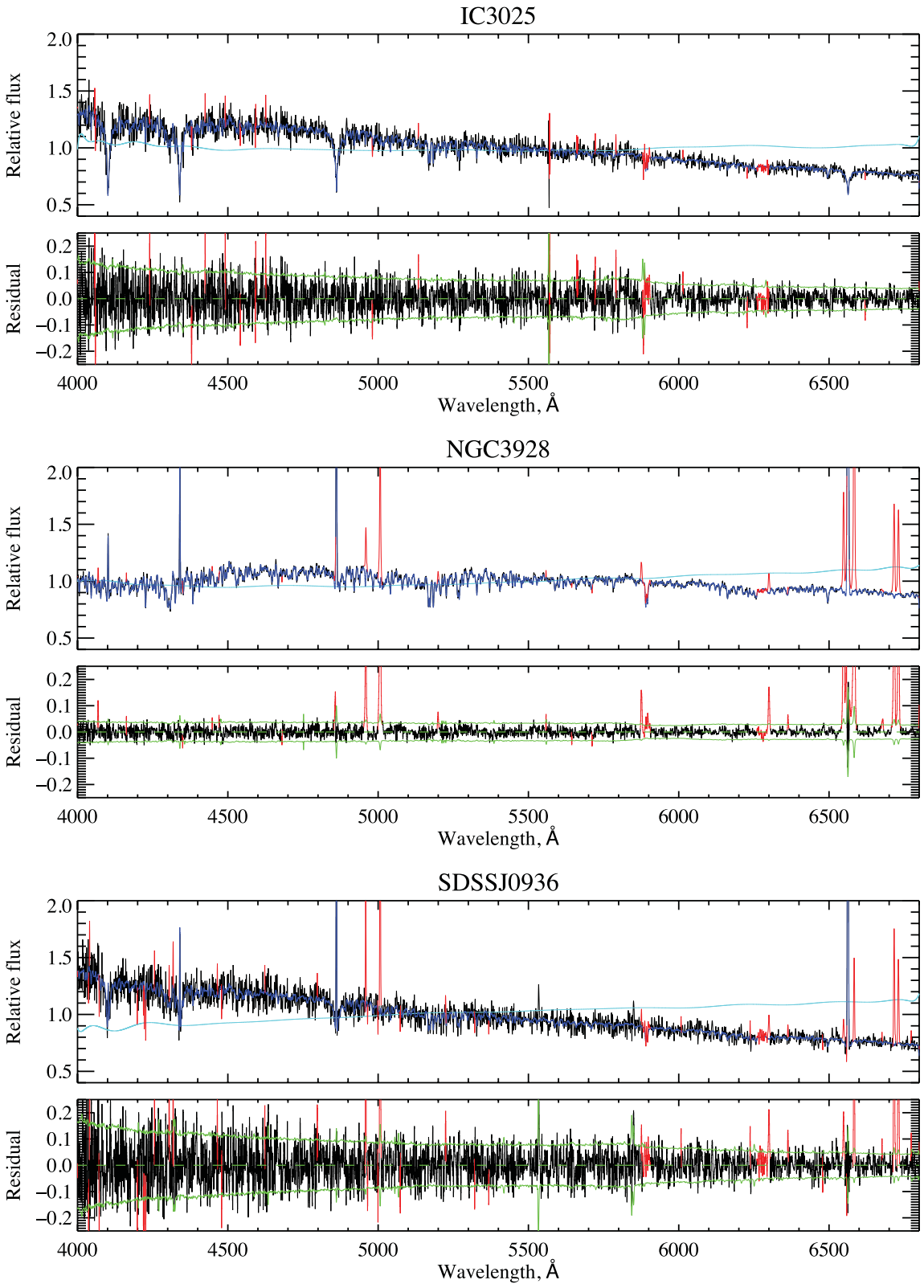

Figure A1 – *continued*

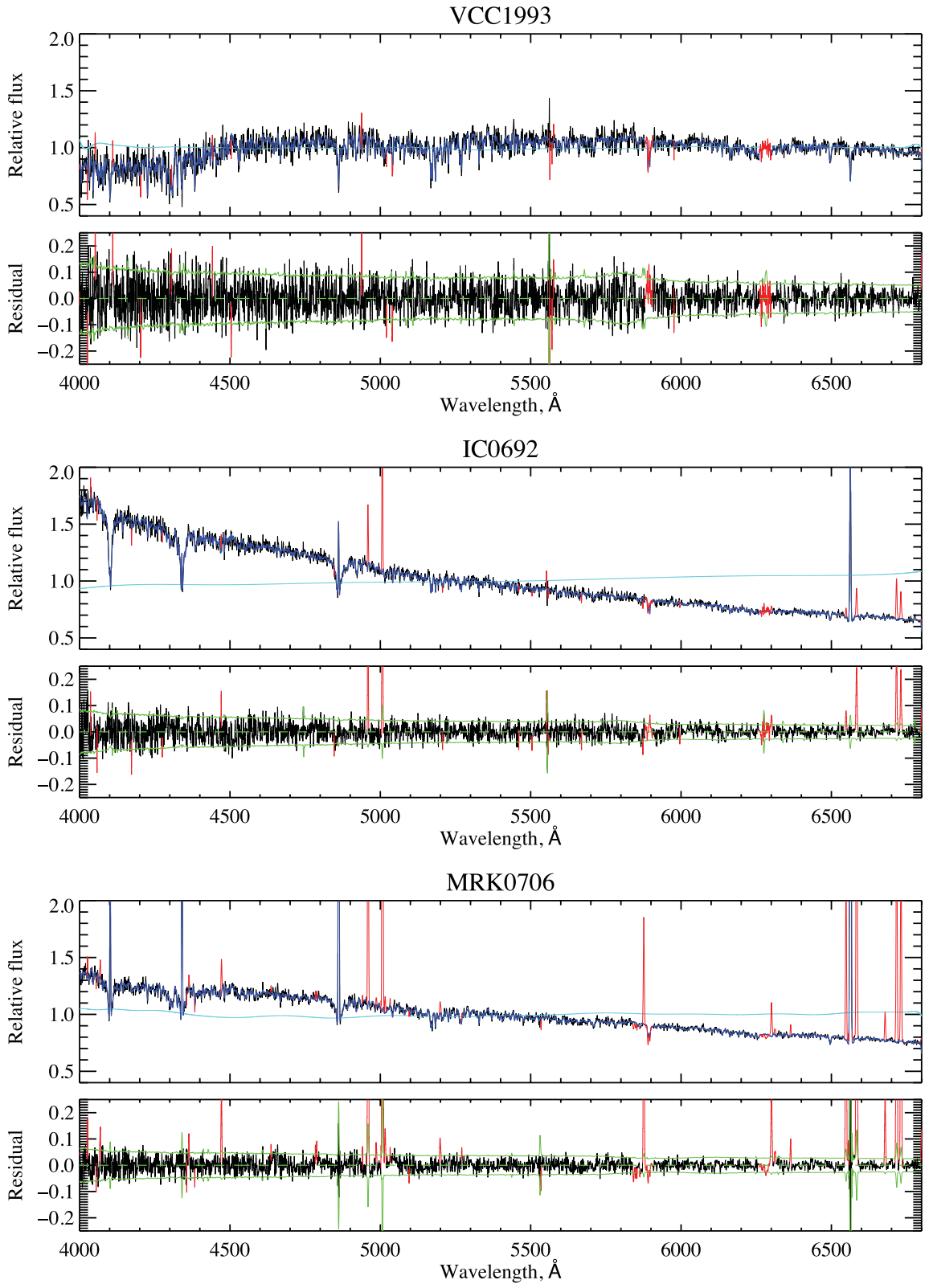

Figure A1 – *continued*

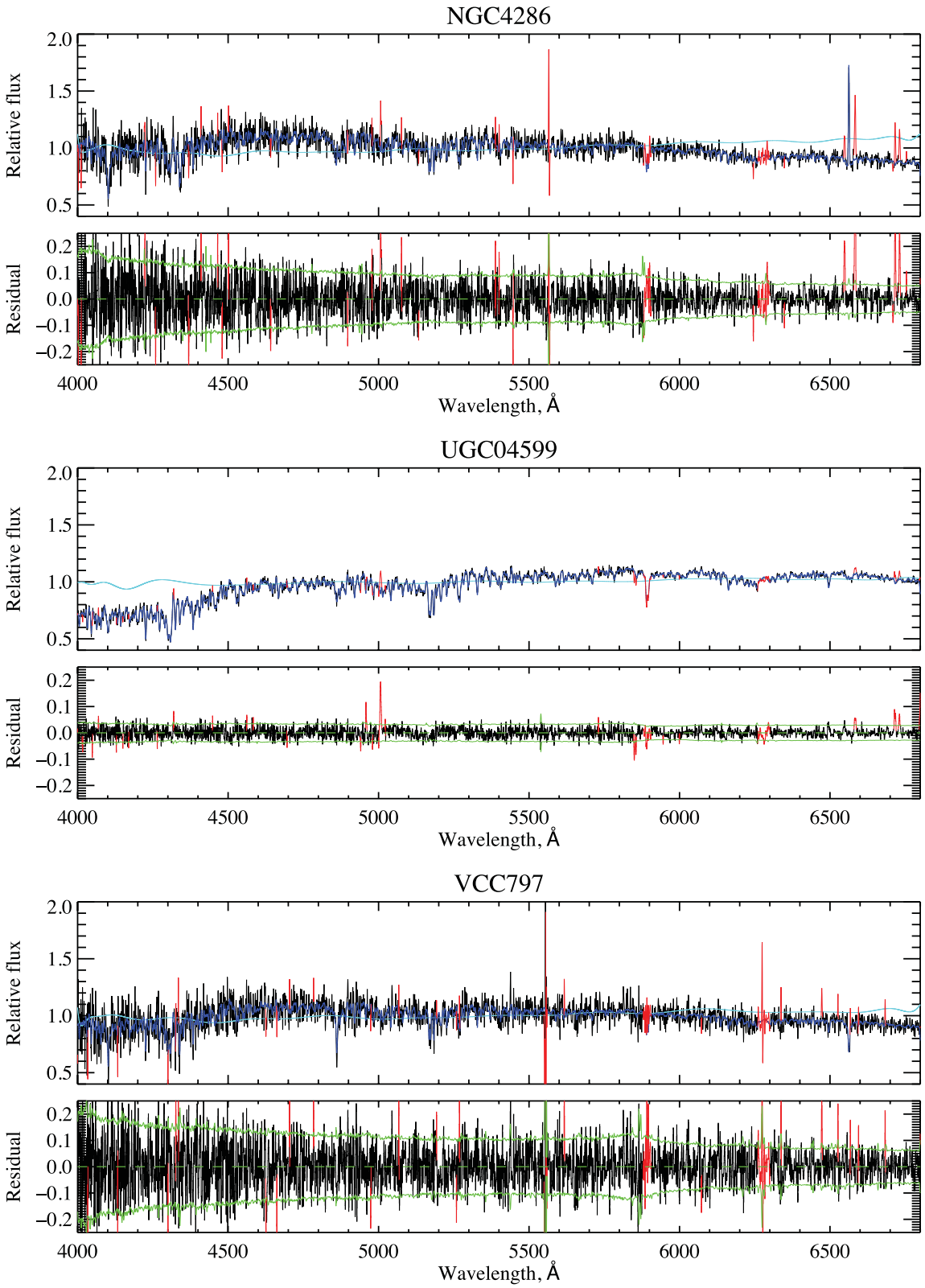

Figure A1 – *continued*

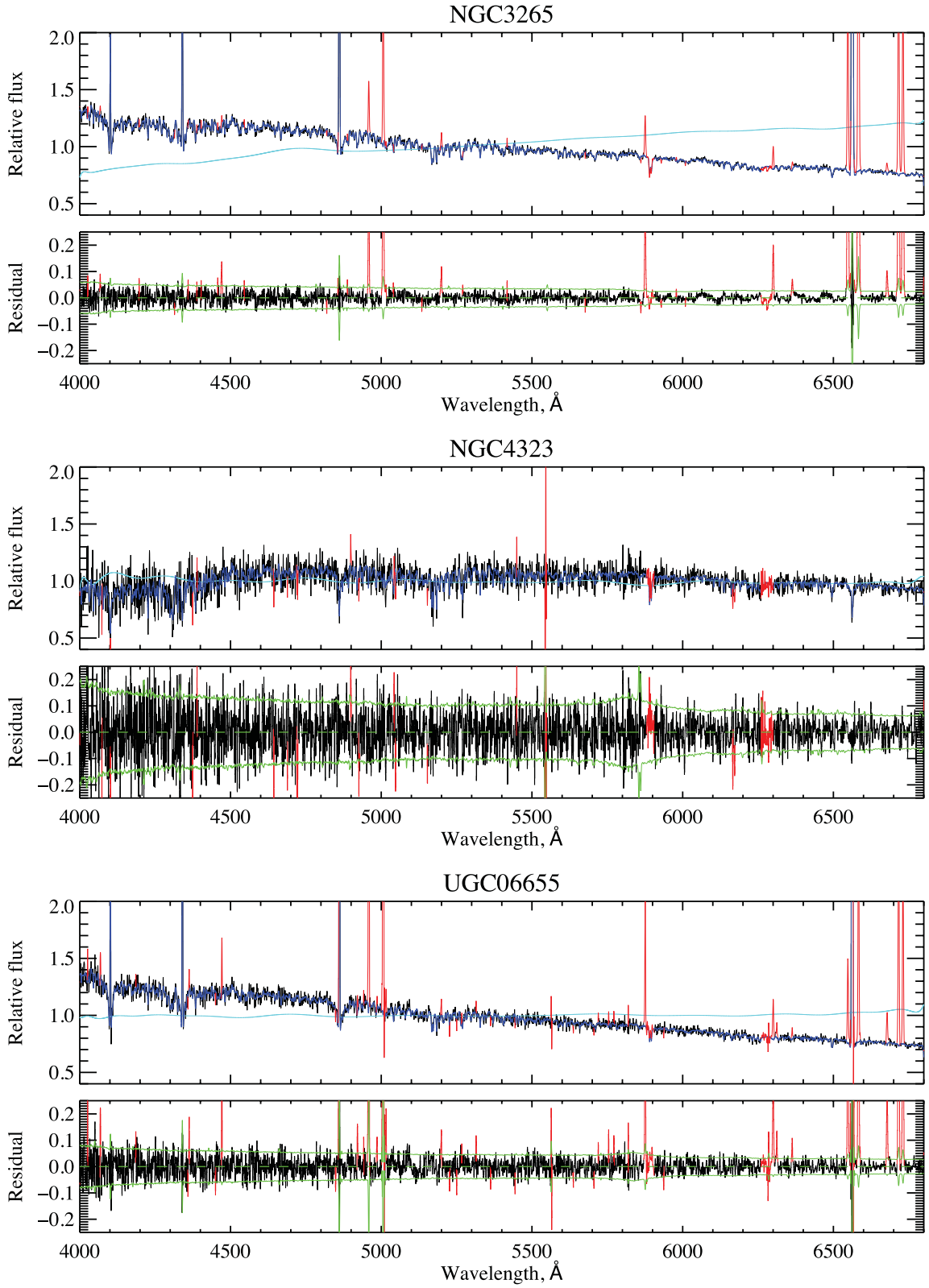

Figure A1 – *continued*

This paper has been typeset from a TEX/LATEX file prepared by the author.